ANALYZING THE RETRIEVAL ACCURACY OF OPTICALLY ACTIVE WATER COMPONENTS FROM SATELLITE DATA UNDER VARYING IMAGE RESOLUTIONS

F. Sunar[1], A. Dervisoglu[1], N. Yagmur[2], E. Aslan[3], M. Ozguven[4]

[1] ITU, Civil Engineering Faculty, Geomatics Engineering Department, 34469 Maslak, Istanbul, Turkiye
(fsunar, adervisoglu)@itu.edu.tr
[2] Gebze Technical University, Engineering Faculty, 41400 Kocaeli, Turkiye – nyagmur@gtu.edu.tr
[3] TUBITAK MRC Marine and Coastal Research Group, Kocaeli, Turkiye
(ertugrul.aslan)@tubitak.gov.tr
[4] Pixmars Technology, Istanbul, Turkiye – ozguven@pixmars.com

KEY WORDS: Water Quality, Gulf of Izmit, Sentinel-2, PlanetScope, Spatial Mapping

ABSTRACT:

Water quality monitoring has a key role in maintaining a sustainable ecosystem and environmental health. To ensure consistent monitoring, remote sensing provides regular data acquisition with varying spatial resolutions. However, more accurate, and effective solutions can be achieved by integrating remote sensing data with in-situ measurements. This study investigates the integration of in-situ measurements with satellite data, which have different spectral and spatial resolutions, using linear and exponential regression models for four optically active components in the Gulf of Izmit. In this context, Sentinel-2 (S2) and PlanetScope SuperDove (PS) multispectral images, which were acquired on the same date, were used for the comparative analysis of the accurate mapping of chlorophyll-a (Chl-a), turbidity, Secchi disk depth (SDD) and total suspended matter (TSM) water quality parameters combined with simultaneously collected in-situ measurements. The models were evaluated using validation data, along with visual comparison, to assess their accuracy. The results indicate that, overall, exponential models provide more accurate results than linear models, except for the SDD parameter. Furthermore, models created with S2 data demonstrate better performance in retrieving water quality parameters for Chl-a, turbidity, and TSM, with R^2 values of 0.71, 0.84, and 0.91, respectively. The linear model created with PS data stands out in the accurately mapping of SDD parameter. Nevertheless, the spatial distribution of these parameters using both satellite dataset exhibits a similar pattern throughout the gulf, which is under threat from significant terrestrial pollution sources, particularly in the eastern part.

1. INTRODUCTION

Water quality, encompassing the physical, chemical, and biological characteristics of water such as temperature, dissolved oxygen levels, nutrient content, and the presence of pollutants, is a critical aspect of environmental health and can affect the well-being of both humans and aquatic life (EPA, 2021; UNEP, 2020). There exist numerous concerns regarding water resources, including urbanization and industrialization, which pose significant threats to water quality (Ano and Okwunodulu, 2008; Adeniyi and Ighalo, 2019). Thus, the retrieval of water quality parameters becomes imperative as it enables us to monitor and evaluate the health of water bodies, identify potential sources of contamination, and make management decisions about the use and protection of water resources.

Water quality parameters can be retrieved through a variety of methods, including in-situ monitoring, remote sensing, and laboratory analysis. In-situ measurements and laboratory analysis of water samples are point based monitoring methods and it is difficult to consistently collect in-situ data due to the need of time, labour, and financial support. However, remote sensing provides a cost-effective and non-invasive method for measuring water quality parameters such as chlorophyll-a, turbidity, and dissolved organic matter (Sunar et al., 2022; Sunar et al., 2023). Additionally, they offer a synoptic view of water bodies, enabling the detection of variations in water quality across wide areas, and frequent measurements over time help to monitor temporal changes in water quality. This is particularly useful for monitoring dynamic water systems that experience rapid changes due to natural or human-induced factors (Gomez et al., 2001; Laubach et al., 2016). Along with the numerous advantages it offers, remote sensing data makes it possible to effectively monitor water body dynamics at various spatial and temporal scales (Hu et al., 2022; Zhu et al., 2022; Muller-Karger et.al., 2018). In this context, the integration of in-situ measurements and remote sensing techniques is essential to effectively map water quality parameters, improve our understanding of their distribution, and assess the state of water bodies. With this integration, models can be developed to enhance our scientific knowledge and provide accurate insights into water quality (Gholizadeh et al., 2016).

There are various studies that used multiple satellite images having low (Hu, 2022), medium (Niroumand-Jadidi et al., 2022; Caballero et al., 2022), and high (Mortula et al., 2020; Duan et al., 2023) spatial resolution in the monitoring of water quality parameters and organic matters like mucilage. For the water quality monitoring of large water bodies, low spatial resolution satellite images (i.e., MODIS, MERIS, Sentinel-3 OLCI) provide effective solutions with high coverage and daily temporal resolution; however, their spatial resolutions are not sufficient for the mapping gulfs, coastal regions, and small water bodies. With that purpose, medium and high spatial resolution satellite images (i.e., Landsat, Sentinel-2, Worldview, PlanetScope, etc.) are preferred in the water quality analysis of these regions. Landsat and Sentinel-2 satellite images have been widely preferred due to the freely availability. However, high resolution satellite images are needed to map the distribution of water quality parameters of small water bodies, gulfs, lagoons, and coasts due to providing more detail with smaller coverage area (Niroumand-Jadidi et al., 2020; Wirabumi et al., 2021).

Retrieving active water quality parameters using optical satellite images involves a multi-step process. Initially, the satellite images must undergo pre-processing to eliminate atmospheric influences and convert raw reflectance data into meaningful

information related to water quality. Subsequently, it becomes necessary to identify and extract the specific bands within the satellite images that are sensitive to optically active water components (OACs) such as Chlorophyll-a (Chl-a) or Secchi disk depth (SDD). After identifying the relevant bands, empirical or semi-empirical algorithms are applied to derive the distribution of the considered water quality parameters. These algorithms are typically based on statistical models that have been developed using in-situ measurements of the water quality parameters. Finally, the accuracy of the retrieved water quality parameters needs to be validated by comparing them with in situ water measurements. Despite its limitations, retrieving optically active water quality components from optical satellite images is a valuable method for monitoring water quality on a broad scale and has several uses in environmental management and decision-making (Lu and Weng, 2007; Son et al., 2013; Muller-Karger et al., 2018).

This study builds upon the work done in 2022 and aims to evaluate the spatial distribution of water quality parameters, including Chl-a, turbidity, SDD, total suspended matters (TSM) and, which are OACs in the inner reservoir of the Gulf of Izmit. To achieve this, two different satellite datasets (Sentinel-2 (S2) and PlanetScope (PS) satellite images) and in-situ water samples were used. To establish the relationship between the in-situ measurements and satellite images, in-situ data was collected at the same date as the satellite image. Bivariate linear and exponential regression models were established and results were evaluated with accuracy metrics and visual interpretation.

Since there is a paucity of literature on the utilization of Planetscope SuperDove image data in the analysis of inland water quality, this study focuses on examining its effectiveness by conducting a comparative analysis with Sentinel-2 data.

2. STUDY AREA

The Gulf of Izmit, situated in the eastern part of the Sea of Marmara within the north-western region of Turkey, is characterized by three distinct regions: the western, central, and eastern (inner) parts. With a total length of 49 kilometres and a variable width ranging from 2 to 10 kilometres, the gulf exhibits different depth profiles in each region. The western part features depths of approximately 200 meters, the central region has an average depth of around 180 meters, and the eastern (inner) region is characterized by shallower depths, approximately 35 meters (Güven and Ünlü, 2000).

With an area of around 310 km^2, the Gulf of Izmit has been an important centre of commerce and trade for centuries with its many major ports. However, the Gulf of Izmit has experienced environmental degradation due to industrial and urban development, as well as pollution from agriculture and shipping activities, particularly in the eastern part. Therefore, the inner reservoir of Izmit Bay has received particular attention in this research since it has recently been the focus of environmental concerns (Aral and Gürel, 2004; Ozhan, 2004; Tarkan, 2012; Tarkan et al., 2013).

The location of the study area is given in Figure 1. White points show the samples that were used for the model establishment and red points are the validation samples.

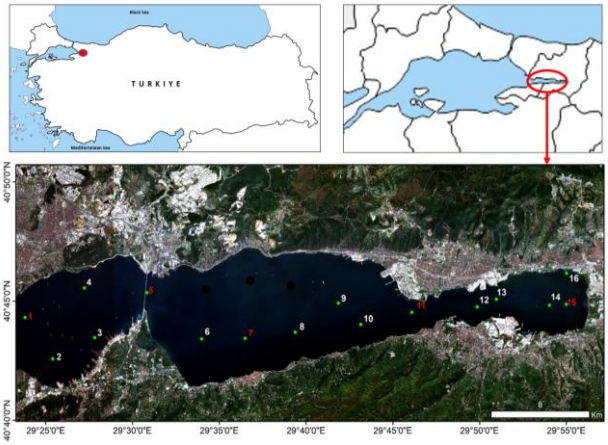

Figure 1. Map of the study area and locations of collected in-situ samples.

3. MATERIALS AND METHODOLOGY

For this study, S2 and PS satellite images acquired on October 26, 2022, were utilized. The S2 satellite images are freely provided by the European Space Agency and the Bottom-of-Atmosphere (BOA) image was chosen for the image analysis. The spatial resolution of S2 varies between 10 to 60 m; however, the used satellite data was resampled to the 10 m.

The PS images utilized in this study were acquired by PS2. The PS SuperDove satellite imagery, which is openly accessible, was utilized for educational purposes in this research. These images were subjected to atmospheric correction to convert them to surface reflectance data obtained using the 6SV2.1 radiation transfer code 8 (Planet, 2023). Table 1 presents a comparison of the main features between the PS and S2 satellites. The S2 satellite image comprises 13 bands, but for the regression analysis to assess the performance of both satellites in the same wavelength coverage, only 8 bands from the S2 satellite were used. Moreover, in this study, two PS image frames were employed due to their comparable coverage to a single S2 image frame over the Gulf of Izmit.

Along with two satellite data, 16 in-situ water samples were collected simultaneously. Out of these 16 measurements, 11 were utilized in the regression analysis, while the remaining five were reserved for accuracy assessment purposes. The in-situ water samples were collected on the same date as the satellite data, which was October 26, 2022.

Bivariate linear and exponential regression analyses were conducted separately in this study using in-situ water quality samples and two satellite images. Linear regression involves modelling the relationship between two variables by fitting a linear equation to the observed data. One variable is considered the independent variable, while the other variable serves as the dependent variable. Conversely, exponential regression is a statistical technique employed to determine an equation that represents an exponential relationship between a dependent variable and one or more independent variables. It is a curve fitting method that aims to identify the exponential function that best fits a given set of data points. Like linear regression, exponential regression is extensively utilized in biology, physics, and other scientific domains to model and predict exponential relationships, making it a valuable technique for analysing available data.

Main features	PS	S2
Spatial resolution	3-m	10-m / 20-m / 60-m
Spectral resolution	8 bands Coastal Blue: 431-452 Blue: 465-515 Green: 513-549 Green II: 547-583 Yellow: 600-620 Red: 650-680 Red-Edge: 697-713 NIR: 845-885	13 bands Coastal Blue:433- 453 Blue: 458-523 Green: 543-578 Red: 650-680 Red-Edge (RE1): 698-713 Red-Edge (RE2): 733-748 Red-Edge (RE3): 773-793 NIR: 785-899 NIR Narrow: 855-875 Water Vapour: 935-955 SWIR Cirrus: 1360-1390 SWIR1: 1565-1655 SWIR2: 2100-2280
Radiometric resolution	11-bit	12-bit
Temporal resolution	Daily	10 days with each satellite five days with (S2A & 2B)
Orbit height	475 km	786 km
Orbit inclination	≈ 98^0	98.62^0

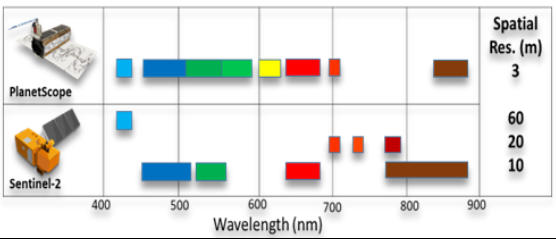

Table 1. Key characteristics of PS and S2 satellites (Planet, 2023).

Both regression methods aim to determine the optimal values of the equation's constants that minimize the disparity between predicted values and actual data points. This is commonly achieved through the method of least squares, which minimizes the sum of squared differences between predicted and observed values. However, it is important to note that linear regression is sensitive to data outliers, which can significantly impact its performance and lead to models with reduced accuracy (Kiernan, 2014).

Several models were developed to establish relationships between water quality samples and selected relevant band combinations using both linear and exponential regression analysis. These models were initially evaluated based on criteria such as the coefficient of determination (R^2), standard error, and F value. Models with high R^2 values were then applied to the satellite images, in conjunction with a visual inspection process. Finally, the visually best-performing models were assessed using test samples, utilizing accuracy metrics such as Root Mean Square Error (RMSE) and Mean Absolute Error (MAE).

4. APPLICATION AND RESULTS

Linear and exponential regression were employed using 11 training in-situ samples, and the spectral response of these samples was collected from satellite data for the Chl-a, turbidity, SDD, and TSM water quality parameters. The best-performing models, determined both visually and statistically, were identified for each parameter. These models, along with their corresponding statistical measures, are presented in Table 2.

Parameter	Data	Band Comb.	Model Equation	R^2	Std. Error	F
Chl-a	**S2**	**B5–B4**	$y=1.7144e^{410.73x}$	**0.71**	0.84	21.98
	PS	B8×B2	$y=1.3312e^{1453.5x}$	0.46	1.14	7.77
Turbidity	**S2**	**B5–B4**	$y=0.2341e^{259.84x}$	**0.84**	0.37	46.20
	PS	B8×B2	$y=0.2074e^{855.88x}$	0.42	0.69	6.38
SDD	S2	B2/B3	y=83.305x-76.604	0.54	1.76	10.74
	PS	**B8×B2**	y=-3471.4x+8.6154	**0.83**	1.08	43.54
TSM	**S2**	**B5-B4**	$y=1.7076e^{324.99x}$	**0.91**	0.33	89.75
	PS	B8×B2	$y=1.4591e^{1080.4x}$	0.46	0.80	7.63

Table 2. Best-performing models for water quality parameters (Chl-a, Turbidity, SDD, and TSM) using datasets from two satellites.

As seen in Table 2, the examination of the results reveals that, in general, the utilization of exponential models for retrieving water quality parameters yielded relatively better outcomes when evaluating the goodness-of-fit through measures such as R^2, standard error, and F-test statistics. For the S2 satellite, in the regression analysis, the (B5-B4) band combination performed well in reflecting the distribution of water quality parameters, except for the SDD parameter. However, it is noteworthy that when considering the PS satellite images, the (B8×B2) band combination significantly outperformed the other models used, particularly for the SDD parameter. Although the (B2/B3) band combination of the S2 image yielded the best model results for the SDD parameter, the obtained R^2 value was relatively low (0.54), as observed.

In this study, similar findings were observed as in the study conducted by Wirabumi et al. (2021), which highlights that for mapping TSM and turbidity using PS data, the red (B5) and NIR (B8) bands play a prominent role in shallow water, while as the water deepens, the blue (B2) band can significantly complement the red band, NIR band, or both. Despite the (B8×B2) combination demonstrating the best performance for TSM and turbidity estimation using PS data, the obtained R^2 values were lower than expected at 0.46 and 0.42, respectively.

The models presented in Table 2 were assessed using accuracy metrics (RMSE and MAE) on five validation samples for each parameter. The results are detailed in Table 3. The analysis demonstrates that, overall, the exponential models yielded better results, and the performance of S2 satellite data surpassed that of PS data in retrieving water quality parameters, except for the SDD parameter. Interestingly, in contrast to the other three parameters, linear modelling demonstrated higher accuracy for both data sources in the thematic mapping of the SDD parameter. Additionally, when estimating the SDD parameter, the PS data showed higher R^2 values (0.83 compared to 0.54) and lower RMSE and MAE errors (1.15 compared to 1.39 and 1.08 compared to 0.96, respectively) compared to the S2 data.

Following the accuracy assessment, the models were individually applied to the satellite images for each parameter to visually compare the results. The thematic maps representing each parameter are presented in Figure 2. It is evident that the

spatial distribution depicted in the maps derived from the PS satellite image appears smoother compared to those derived from the S2 satellite image. Nevertheless, overall, the thematic maps for the parameters exhibit a similar distribution pattern throughout the gulf.

Based on visual analysis of the maps and photographs taken during the in-situ measurements (Figure 3), higher concentrations of Chl-a were observed in the inner part of the Gulf and the coastal regions. As observed, the S2 model exhibits better performance than the PS model, as indicated by a higher R^2 coefficient of 0.71. The distribution patterns and R^2 coefficient differences for the TSM parameter exhibit similarity to those observed for the Chl-a distribution in both datasets, indicating the influence of common factors such as water currents, sedimentation, pollution sources, and biological activities within the gulf. Furthermore, in the TSM models, the S2 model displayed higher accuracy than the PS model, as evidenced by its higher R^2 value of 0.91 compared to 0.46. In the maps depicting turbidity, the S2 model demonstrates superior accuracy compared to the PS model, achieving R^2 values of 0.84 and 0.42, respectively.

In general, the eastern coastal part of the Gulf of Izmir displayed higher concentrations of Chl-a, turbidity, and TSM, while exhibiting lower SDD values, as illustrated in Figure 2. These observations are consistent with previous research studies indicating a high level of eutrophication in the eastern region (Okay et al., 2001; Ediger et al., 2013). Furthermore, the fluctuations in the visual characteristics of the water during sampling measurements, as depicted in Figure 3, support the degradation of water quality along the eastern coast. These observations reinforce the understanding that the eastern part of the region is subject to significant terrestrial pollution, primarily originating from domestic and industrial waste, as well as the influx of pollutants through streams into the gulf (Eyuboglu and Eyuboglu, 2020).

Parameter	Variables	Regression Type	Data	R	R^2	RMSE	MAE
Chl-a (mg/m^3)	B5-B4	Exponential	S2	0.84	0.71	2.21	1.90
	B8×B2	Exponential	PS	0.68	0.46	3.19	2.22
Turbidity (NTU)	B5-B4	Exponential	S2	0.92	0.84	0.17	0.14
	B8×B2	Exponential	PS	0.64	0.42	0.20	0.13
SDD (m)	B2/B3	Linear	S2	0.74	0.54	1.39	1.08
	B8×B2	Linear	PS	0.91	0.83	1.15	0.96
TSM (mg/l)	B5-B4	Exponential	S2	0.95	0.91	1.15	0.98
	B8×B2	Exponential	PS	0.68	0.46	1.70	1.28

Table 3. Best-performing models for each parameter using datasets from two satellites.

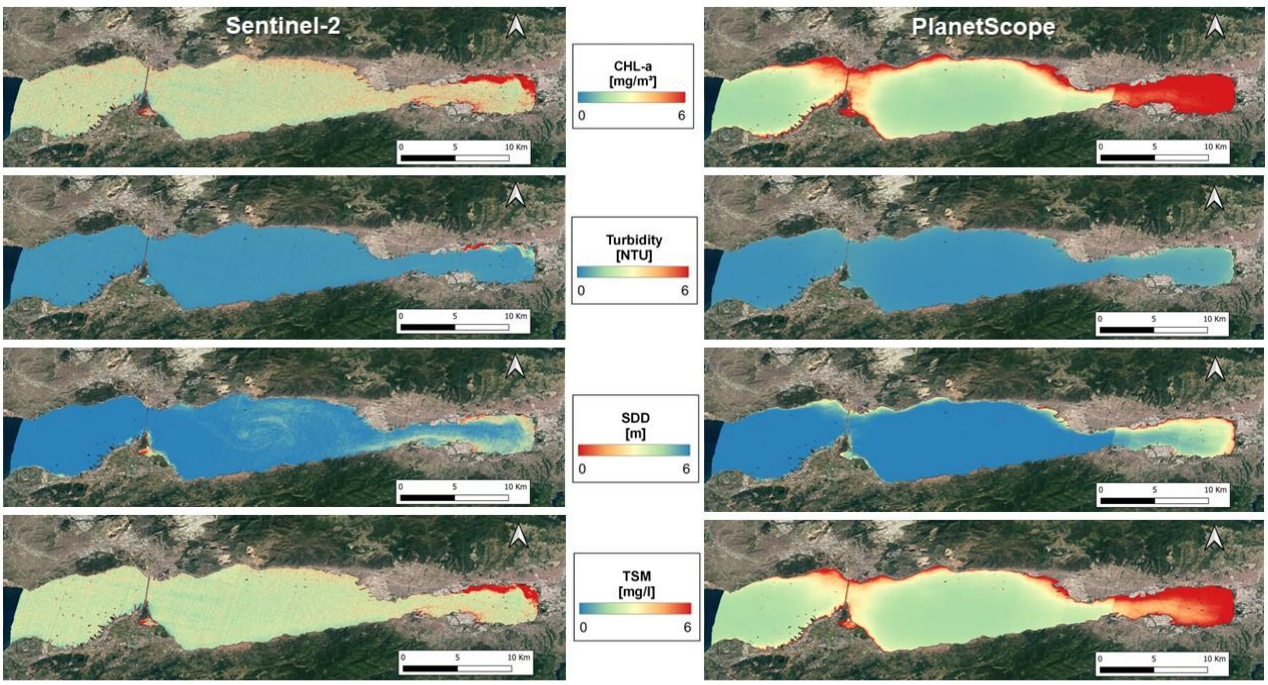

Figure 2. Thematic maps depicting the distribution of four water quality parameters (Chl-a, Turbidity, SDD, and TSM) derived from the best models.

Figure 3. Variations in the visual characteristics of water bodies observed in the Gulf of Izmir during the sampling measurements.

5. CONCLUSION

In this study, two different satellite datasets were utilized to retrieve and map the concentrations of key OACs, namely Chl-a, turbidity, SDD, and TSM. As demonstrated, the regression model based on the B5-B4 bands has exhibited efficiency in spatially mapping OACs using S2 data, yielding higher R^2 values (0.71, 0.84, and 0.91) for Chl-a, turbidity, and TSM parameters, respectively. Conversely, the best performing models using PS data were observed to be created with the B8×B2 band combination, specifically for SDD mapping, resulting in an R^2 value of 0.83.

In general, the performance of PS data for the retrieval of the four parameters was found to be less accurate than that of S2. The lower performance of PS could be attributed to the difference in spectral resolution between the two sensors. Despite its primary design for land applications, the S2 satellite data demonstrated effectiveness in detecting and mapping water quality parameters such as Chl-a, SDD, and turbidity, benefiting from its higher spectral resolution. In contrast, PS does not have as many dedicated bands for water quality measurements, even though it has a higher spatial resolution than S2. Therefore, it can be concluded that freely provided S2 data has shown efficiency in the thematic mapping of OACs in the Gulf of Izmir. However, considering its limited coverage area and higher cost, PS data may be more suitable for detailed mapping of OACs in highly fragile areas within the inner part of the gulf.

Future work will focus on investigating seasonal and annual trends and changes of not only the four parameters used in this study but also other optically active and inactive parameters. This will contribute to a more comprehensive understanding of water quality variations over time.

ACKNOWLEDGEMENTS

This work has been supported by the "Integrated Marine Pollution Monitoring 2020-2022 Programme" carried out by the Ministry of Environment, Urbanization and Climate Change/General Directorate of EIA, Permit and Inspection/ Department of Laboratory, Measurement and coordinated by TUBITAK- MRC ECPI. Additionally, the authors would like to express their gratitude to Planet Labs Inc. for their valuable educational support in providing access to Planet Scope data.

REFERENCES

Adeniyi, A.G., Ighalo, J.O., 2019. Biosorption of pollutants by plant leaves: an empirical review. *Journal of Environmental Chemical Engineering*, 7(3), 103100.

Ano, A.O., Okwunodulu, F.U., 2008. Effect of population and level of industrialization on underground water quality of Abia state, Nigeria-physico-chemical properties. *African Journal of Biotechnology*, 7(4).

Aral, O., Gürel, A., 2004. Sources of pollution in the Gulf of Izmit and their impacts on the environment. *Environment International*, 30(6), 743-755.

Caballero, I., Roca, M., Santos-Echeandía, J., Bernárdez, P., Navarro, G., 2022. Use of the Sentinel-2 and Landsat-8 Satellites for Water Quality Monitoring: An Early Warning Tool in the Mar Menor Coastal Lagoon. *Remote Sensing*, 14(12), 2744.

Duan, P., Zhang, F., Liu, C., Tan, M.L., Shi, J., Wang, W., Cai, Y., Kung, H.T., Yang, S., 2023. High-resolution PlanetScope Imagery and Machine Learning for Estimating Suspended Particulate Matter in the Ebinur Lake, Xinjiang, China. *IEEE Journal of Selected Topics in Applied Earth Observations and Remote Sensing*. Vol.16, 1019-1032.

Ediger, D., Beken, Ç., Tolun, L., Tüfekçi, V., 2013. İzmit Körfezi Su Kalitesinin ve Karasal Girdilerin İzlenmesi ve Kirliliğin Önlenmesine Yönelik Önerilerin Geliştirilmesi Projesi Sonuç Raporu, Technical Report, TÜBİTAK MAM Çevre Enstitüsü, Gebze, Kocaeli. (in Turkish)

EPA, United States Environmental Protection Agency, 2021. Water Quality. Retrieved from https://www.epa.gov/waterquality

Eyuboglu, H., Eyuboglu, O., 2020. İzmit Körfezi'nde Kirletici Kaynakların Dağılımı ve Deniz Ekosistemine Etkisi. *Journal of Anatolian Environmental and Animal Sciences*, 5 (1), 25-37. (in Turkish)

Gholizadeh, M.H., Melesse, A.M., Reddi, L., 2016. A comprehensive review on water quality parameters estimation using remote sensing techniques. *Sensors*, 16(8), 1298.

Gomez, C., White, E., Luvall, J.C., 2001. Advantages and limitations of current and emerging remote sensing data for studies of ecological change along the Gulf Coast. *Remote Sensing of Environment*, 78(2), 339-347.

Güven, K.C., Ünlü, S., 2000. Oil pollution in sea water of Izmit Bay following the earthquake (17 Aug 1999). *Journal of Black Sea/Mediterranean Environment*, 6(3).

Hu, C., 2022. Sea snots in the Marmara Sea as observed from medium-resolution satellites. IEEE Geoscience and Remote Sensing Letters, 19, 1-5.

Hu, M., Ma, R., Xiong, J., Wang, M., Cao, Z., Xue, K., 2022. Eutrophication state in the Eastern China based on Landsat 35-year observations. *Remote Sensing of Environment*, 277, 113057.

Kiernan, D., 2014. Natural resources biometrics. Open SUNY Textbooks, Milne Library, State University of New York at Geneseo.
https://milnepublishing.geneseo.edu/natural-resources-biometrics/

Laubach, J., Rücker, J., Graf, W., 2016. Large-scale monitoring of suspended sediment in river basins with remote sensing: a review. Wiley Interdisciplinary Reviews: *Water*, 3(3), 383-402.

Lu, D., Weng, Q., 2007. A survey of image classification methods and techniques for improving classification performance. *International Journal of Remote Sensing*, 28(5), 823-870.

Mortula, M., Ali, T., Bachir, A., Elaksher, A., Abouleish, M., 2020. Towards monitoring of nutrient pollution in coastal lake using remote sensing and regression analysis. *Water*, 12(7), 1954.

Muller-Karger, F.E., Hestir, E., Ade, C., Turpie, K., Roberts, D.A., Siegel, D., Miller, R.J., Humm, D., Izenberg, N., Keller, M., Morgan, F., 2018. Satellite sensor requirements for monitoring essential biodiversity variables of coastal ecosystems. *Ecological Applications*, 28(3), pp.749-760.

Niroumand-Jadidi, M., Bovolo, F., Bresciani, M., Gege, P., Giardino, C., 2022. Water Quality Retrieval from Landsat-9 (OLI-2) Imagery and Comparison to Sentinel-2. *Remote Sensing*, 14(18), 4596.

Niroumand-Jadidi, M., Bovolo, F., Bruzzone, L., Gege, P., 2020. Physics-based bathymetry and water quality retrieval using planetscope imagery: Impacts of 2020 COVID-19 lockdown and 2019 extreme flood in the Venice Lagoon. *Remote Sensing*, 12(15), 2381.

Okay, O.S., Tolun, L., Telli-Karakoç, F., Tüfekçi, V., Tüfekçi, H., Morkoç, E., 2001. İzmit Bay ecosystem after Marmara earthquake and subsequent fire: The long-term data. *Marine Pollution Bulletin*, 42(5), 361-369.

Ozhan, E., 2004. Nutrient dynamics and phytoplankton productivity in Izmit Bay, Turkey. Marine Pollution Bulletin, 49(5-6), 388-395.

Planet, 2023. Planet Imagery Product Specifications. https://assets.planet.com/docs/Planet_Combined_Imagery_Product_Specs_letter_screen.pdf (Accessed June 21, 2023).

Son, N.T., Chen, C.F., Chen, C.R., 2013. Advances in remote sensing for oil spill disaster management: challenges and opportunities. *Journal of Environmental Management*, 129, 98-113.

Sunar, F., Dervisoğlu, A., Yağmur, N., Çolak, E., Kuzyaka, E., Mutlu, S., 2022. How efficient can Sentinel-2 data help spatial mapping of mucilage event in the Marmara Sea?. The International Archives of the Photogrammetry, Remote Sensing and Spatial Information Sciences, 43, 181-186.

Sunar, F., Dervişoğlu, A., Yağmur, N., Aslan, E., Atabay, H., 2023. The Spatial Distribution of Selected Optical Active Components in the Gulf of Izmit Using Bivariate/multivariate Regression Analysis. The International Archives of the Photogrammetry, Remote Sensing and Spatial Information Sciences, 48, 361-366.

Tarkan, A.S., Ozulug, M., Acarli, D., Gürsoy Gaygusuz, Ö., Gaygusuz, Ç., 2013. Macrofauna associated with macroalgae in the Gulf of Izmit (Marmara Sea, Turkey). *Journal of the Black Sea/Mediterranean Environment*, 19(3), 340-352.

Tarkan, A.N., 2012. Environmental impacts of industrial activities in the Gulf of Izmit, Turkey. *Water, Air, and Soil Pollution*, 223(8), 5183-5194.

UNEP, United Nations Environment Programme, 2020. Water Quality. Retrieved from https://www.unep.org/resources/water-quality

Wirabumi, P., Kamal, M., Wicaksono, P., 2021. Determining effective water depth for total suspended solids (TSS) mapping using PlanetScope imagery. *International Journal of Remote Sensing*, 42(15), 5784-5810.

Zhu, X., Guo, H., Huang, J.J., Tian, S., Xu, W., Mai, Y., 2022. An ensemble machine learning model for water quality estimation in coastal area based on remote sensing imagery. *Journal of Environmental Management*, 323, 116187.